Microphone-Based Vibration Sensor for UGS Applications

Qianwei Zhou, *Associate Member, IEEE*, Baoqing Li, Huawei Liu, Shengyong Chen, *Senior Member, IEEE*, and Jingchang Huang

***Abstract*—To be an ideal candidate, seismic sensor for wireless unattended ground sensor (UGSs) applications should have lightweight, low noise, high sensitivity, and energy efficiency. Typically, to cover regions far from source, the best choice will be the coil-over-magnet geophone. Because it is usually heavier than batteries, a lighter one should replace it to further cut the weight of sensor nodes. However, currently available seismic sensors, such as micro-electro mechanical systems (MEMS) accelerometers and molecular-electronic transducers, cannot do the job since they usually consume too much energy to achieve low noise level as well as high sensitivity. This work has designed and tested a new kind of vibration sensor, the vibration-to-sound geophone, which can convert seismic waves into sound physically that can then be detected by an MEMS microphone. By using a battery as its proof mass, the vibration-to-sound geophone 1) has better sensibility than the coil-over-magnet geophone from 20 to 500 Hz and is about 58 times more sensitive at 70 Hz which is more than 60 dBV/m; 2) is very light, half the weight of the coil one; and 3) consumes no more than 726 μW which is more energy-efficient than MEMS accelerometers and molecular-electronic transducers.**

***Index Terms*—Microphone, seismic sensor, sound, unattended ground sensor (UGS), vibration.**

I. Introduction

UNATTENDED ground sensors (UGSs) are unmanned monitoring stations often used for military surveillance, troop movement detection, and target identification [1]. Comparing with sound, image, and infrared signals, seismic waves are less sensitive to Doppler effects, noises coming from various moving parts of vehicles, atmospheric, and terrain variations [2], [3], which makes seismic waves widely employed in UGS. To detect seismic targets in UGS, the coil-over-magnet geophone will be the best choice traditionally [4]–[8]. The geophone brings many benefits such as 0 energy consumption, high sensibility, and low noise. However, a lighter one should replace the coil-over-magnet geophone to further cut the weights of sensor nodes, making them air deployable, since the coil one weighs more than 50 g where battery is only 30 g in our UGS system. Although, micro-electro mechanical systems (MEMS) accelerometer is a good candidate [1], [9]–[13], it suffers from high energy consumption, more than 70 mW for low noise version such as SF1500 [10]. Other energy-efficient MEMS accelerometers, such as analog devices ADXL206 MEMS accelerometer (3.5 mW) [14], have the lowest noise density of 110 μg/Hz$^{1/2}$ among AD analog accelerometers, its noise level still higher than 1.2851 μg/Hz$^{1/2}$ at 100 Hz which is measured from our field experiment by the coil-over-magnet geophone. While molecular-electronic transducers [15], [16] are sensitive enough, they are usually too energy expensive to use battery power.

Since there is no sign of any commercially available sensors can do the job, a redesign of the coil-over-magnet geophone may bring us a new kind of senor which is significantly lighter than the coil-over-magnet geophone with similar seismic target detect ability. The ideal newly designed sensor, as a replacer of the coil-over-magnet geophone, has the following characteristics.

1) Its sensibility is higher than 16 dBV/(m/s) from 10 to 500 Hz.
2) It is lighter than 50 g.
3) Its energy consumption is close to 0 or less than 3.5 mW at least.
4) It resonates at low frequency such as 10 Hz or a little higher.

The definition of the sensor frequency range is mainly based on following two reasons: first, the generation and propagation of the seismic waves will filter out the low and high frequency components of the vibration source [8], [17]–[19]; second, the facts observed in field experiments [2]–[4], [7], [8], [20]–[25] that most energy of the typical seismic waves, generated by pedestrians and/or vehicles, are in the band from about 10 to 500 Hz. The coil-over-magnet geophone is, in its simplest form,

Manuscript received September 16, 2016; revised December 24, 2016 and February 9, 2017; accepted February 22, 2017. Date of publication March 14, 2017; date of current version July 10, 2017. This work was supported in part by the National Natural Science Foundation of China under Grants U1509207, 61325019, and 61374094, in part by the Compound Sensor Technology Foundation of China under Grant 6141A01111602, and in part by the Microsystems Technology Key Laboratory Foundation of China under Grant 6142804010203.

Q. Zhou is with the Institute of Computer Vision, College of Computer Science and Technology, Zhejiang University of Technology, Hangzhou 310023, China (e-mail: zhouqianweischolar@gmail.com).

B. Li and H. Liu are with the Shanghai Institute of Microsystems and Information Technology, Chinese Academy of Sciences, Shanghai 200050, China (e-mail: libq@mail.sim.ac.cn; liuhuawei8608@sina.com).

S. Chen is with the College of Computer Science and Technology, Tianjin University of Technology, Tianjin 300384, China, and also with Zhejiang University of Technology, Hangzhou 310023, China (e-mail: sy@ieee.org).

J. Huang is with IBM Research-China, Shanghai 201203, China (e-mail: hjingc@cn.ibm.com).

Color versions of one or more of the figures in this paper are available online at http://ieeexplore.ieee.org.

Digital Object Identifier 10.1109/TIE.2017.2682015

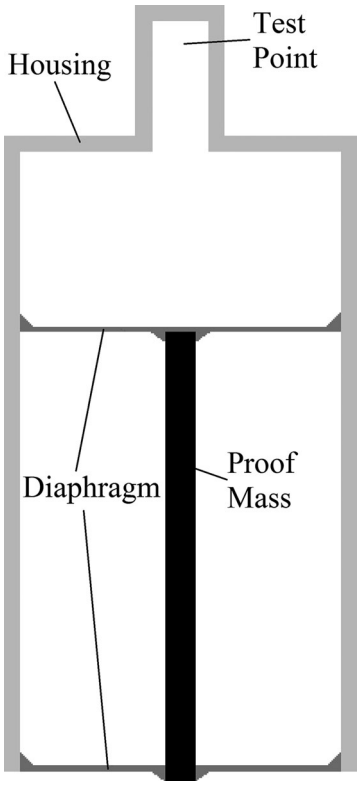

Fig. 1. Cross section of the cylindrical finite-element model of VSG.

just a coil suspended around a permanent magnet [26]. Usually, the permanent magnet accounts for the most parts of weights of the coil-over-magnet geophone. If the moving coil, the proof mass, is not cutting magnetic field lines, instead, it is changing vibrations into another kind of energy form, which can be measured by some other kind of light-weighted sensor, then the permanent magnet could be cut out of the geophone and lead to a lighter geophone.

The idea of the work presented herein, the relationship between vibration and sound is close. Once there are vibrations and air, there are sounds. If an appropriate physical structure can gather and enlarge the generated sound, then a microphone can convert the sound into electronic signal. Since the principle of this geophone is converting vibration into sound, for the convenience of expression, the geophone gets the name vibration-to-sound geophone (VSG). Fig. 1 shows the cross section of the cylindrical finite-element model of a VSG, where the vibration of the housing will change the vertical displacement of the proof mass so as the elastic diaphragms can convert the vibration energy into sound. Once an MEMS microphone is attached to the "test point," the microphone will output voltage signals, which are highly correlated with the incoming seismic waves or vibration signals. To enlarge the generated sound energy, or the magnitude of the air pressure fluctuation in another word, the "test point" should be located in a sealed chamber. As shown in Fig. 1, the housing, the diaphragms, and the proof mass have constituted a sealed chamber with a long neck and air in it all together.

The best VSG we have made currently uses a lithium battery as its proof mass which has been presented in Section III. This VSG is more sensitive than the coil-over-magnet geophone since 20 Hz and is half the weight of the coil one with power consumption less than 726 μW.

This paper is organized as follows. Features of the VSG have been analyzed in theory and simulation in Section II. In Section III, two physical implementations of the VSG have been presented including their transfer function and field test results followed by the conclusion in Section IV.

II. Theory and Simulation

To facilitate the theoretical analysis, the state shown in Fig. 1 is the initial state of the VSG. Since we are interested in the local pressure deviation from the average air pressure of the sealed chamber, air pressures, in and out of the sealed chamber, are initialized as P_0 Pa. In addition, the gravity is not included in the following theory and simulation analysis.

If the touch area between the proof mass and diaphragms is much smaller than the area of diaphragms, and the vertical displacement of the proof mass is small so that diaphragms could react linearly to the displacement, then the relationship between displacements of the proof mass and the ground could be described as follows [9] and the instantaneous state of the sealed chamber could be simplified:

$$\frac{\partial^2 x}{\partial t^2} + 2\lambda\omega_0 \frac{\partial x}{\partial t} + \omega_0^2 x = -\frac{\partial^2 u}{\partial t^2} \tag{1}$$

where u is the displacement of the ground, x is the displacement of the proof mass, ω_0 is the resonant frequency, and λ is the damping factor. The specific values of ω_0 and λ are controlled by many facts such as the value of Young's modulus of the diaphragm, the size of the touch area between the proof mass and the diaphragm, the weight of the proof mass, and so on. In the following analysis, these two variables will be set to several specific values to illustrate the transfer function of the VSG. By Fourier transform, the time derivatives of (1) can be replaced with $i\omega$ [9]. This gives

$$X = \frac{\omega^2}{-\omega^2 + 2i\lambda\omega_0\omega + \omega_0^2} U. \tag{2}$$

As depicted in Fig. 2, when the proof mass moves away from the initial place vertically, it has x meters of displacement along V axis, and the diaphragm together with H axis construct a triangle section which is a cone in three-dimensional reality. Since the cone changes the volume of the sealed chamber, the air pressure in the sealed chamber is highly correlated with the displacement x. Following Boyle's law, the air pressure is given by

$$p = \frac{P_0}{1 + \frac{\pi r^2}{3V_0} x} = \frac{P_0}{1 + \frac{x}{3h_0}} \tag{3}$$

where P_0 is the initial air pressure and V_0 is the initial volume of the sealed chamber, r is the radius of the cone in Fig. 2, and h_0 is the height of the sealed chamber that is a cylinder in its initial state as shown in Fig. 1 and the neck on the top is not included. Since the seismic wave measured by VSG in this work is weak typically, the maximum value of the absolute of x in (3)

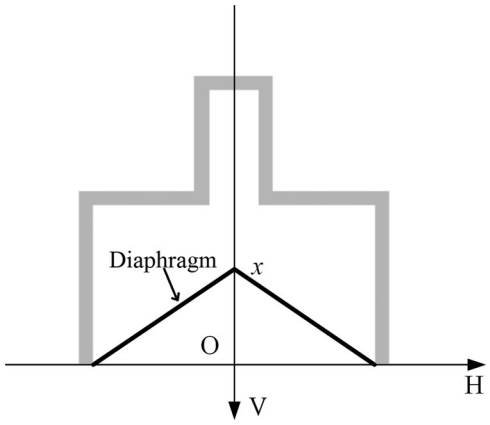

Fig. 2. Simplified instantaneous state of the confined space.

is much less than h_0. Because the absolute value of $x/3h_0$ is much less than 1 and (3) is differentiable around $x = 0$, the first-order approximation of Taylor expansion can be employed to estimate the instantaneous air pressure p as

$$p \approx P_0 - \frac{P_0}{3h_0}x. \tag{4}$$

Keeping the second term of the right of (4), we get the ac component of the instantaneous air pressure $p_{\rm ac}$. Including (2), the Fourier transform of $p_{\rm ac}$ can be written as

$$P_{\rm ac} \approx -\frac{P_0}{3h_0}X = -\frac{P_0}{3h_0}\frac{\omega^2}{-\omega^2 + 2i\lambda\omega_0\omega + \omega_0^2}U. \tag{5}$$

To measure the air pressure, one can put an MEMS microphone at the "test point" as shown in Fig. 1. The MEMS microphone will output the pressure in voltage signal and the Fourier transform of the ac component of the voltage signal can be given by

$$\text{Vol} = S_{\rm mic}P_{\rm ac} \approx S_{\rm mic}\frac{P_0}{3h_0}\frac{-\omega^2}{-\omega^2 + 2i\lambda\omega_0\omega + \omega_0^2}U \tag{6}$$

where $S_{\rm mic}$ is the sensitivity of the MEMS microphone. For ICS-40300 MEMS microphone [27], which has been employed in our field test, its transfer function is almost flat from 6 Hz to 1 kHz. In the following analysis, $S_{\rm mic}$ will be set to the sensitivity of ICS-40300, which is 0.0056 V/Pa typically, P_0 will be set to 1.01325e5 Pa that is the value of the standard atmospheric pressure, and h_0 is 0.0025 m that is the height of the sealed chamber of the VSG sensor we designed for field test. According to (6), different transfer functions can be drawn by setting ω_0 and λ to different values. The amplitude and phase of transfer functions are shown in Fig. 3 where ω_0 is set to 10 or 100 Hz and λ is set to 0.01, 0.1, or 1. The transfer function is flat in high frequency and its sensitivity is about 45 dBV/m at 250 Hz. Since the noise level of ICS-40300 is lower than -140 dBV/Hz$^{1/2}$ [27], the VSG sensor shown in Fig. 3 can detect seismic waves whose amplitude is smaller than 3.1623e – 19 m while the noise we measured in field test by the coil-over-magnet geophone is about 1.0502e – 12 m which means that by careful engineering, the VSG sensor has the potential to replace the coil-over-magnet geophone in UGS systems.

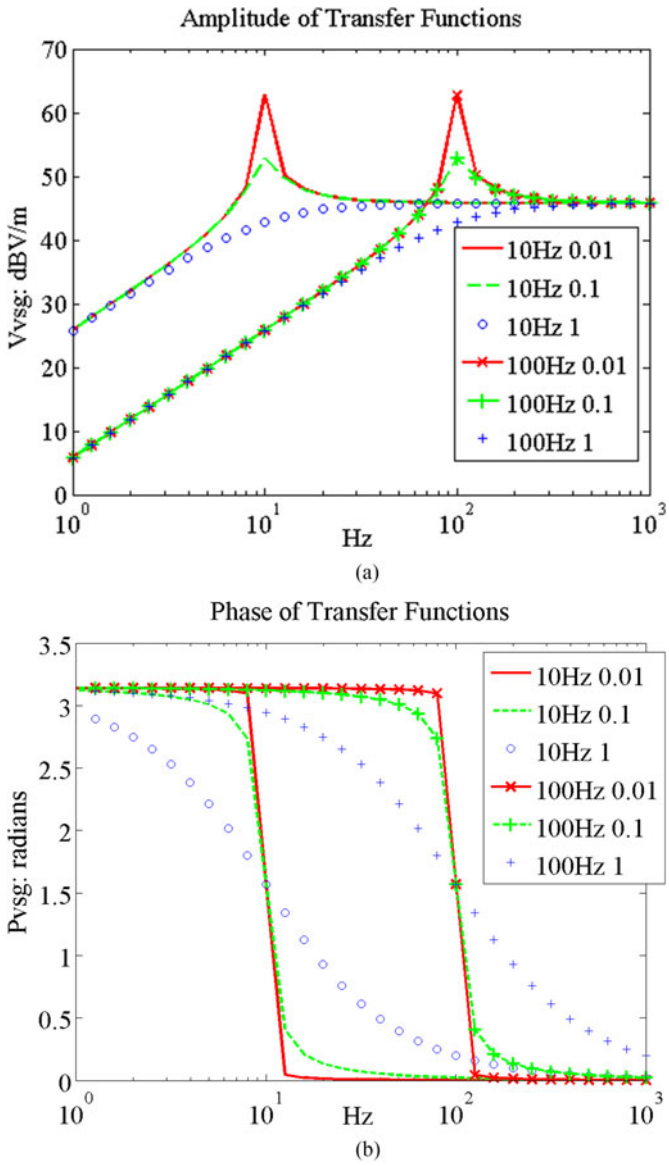

Fig. 3. Transfer functions of VSGs relative to ground displacement.

As shown in Fig. 3, low frequency part of the transfer function is seriously influenced by the values of ω_0 and λ. In this work, numerous finite-element simulations have been conducted to determine the best combination of the radius, thickness, and Young's modulus of the diaphragm, the height of the chamber, the weight of the proof mass, and the touch area between the proof mass and the diaphragm. In Fig. 4, the results of seven of those simulations have been shown and their configurations have been listed in Table I. In Fig. 4, the transfer functions of each configuration have been shown and the frequency range is from 1 to 500 Hz. Although the frequency resolution for simulations 1–5 is 1 Hz and the rest is 2 Hz, we have resampled and linear interpolated them in Fig. 4 for clarity.

From the theoretical analysis, Table I and Fig. 4, five conclusions have been drawn as follows.

1) The resonant frequency of the finite-element model shown in Fig. 1 is mainly controlled by the Young's mod-

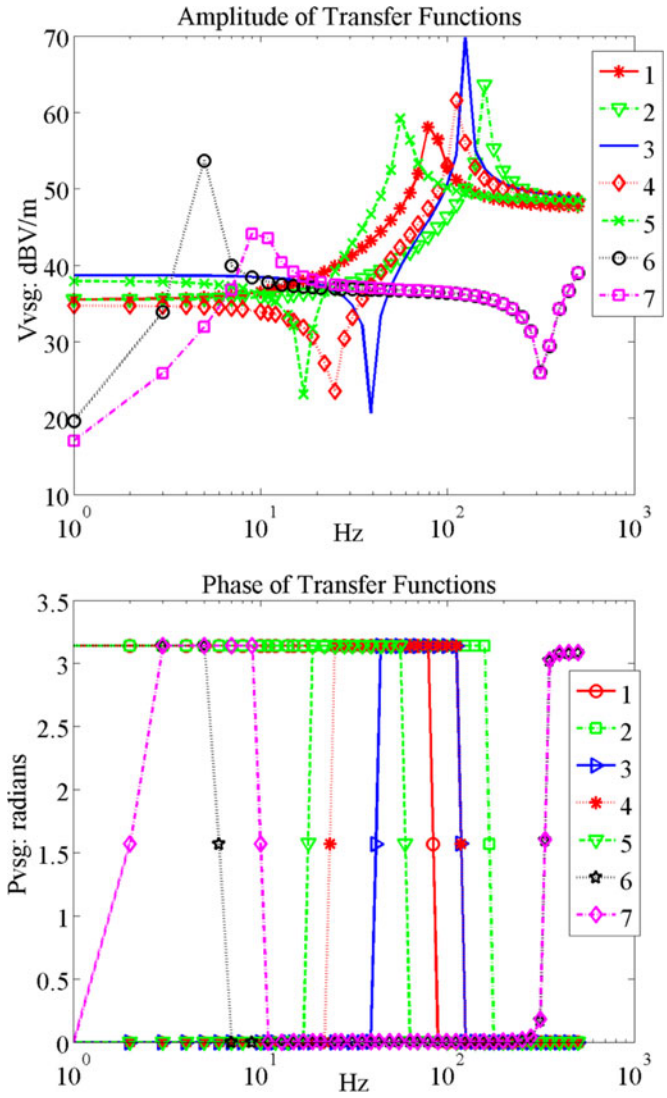

Fig. 4. Results of simulations relative to housing displacement.

TABLE I
PARAMETERS OF SIMULATIONS

Nub.	Radius (mm)	Thickness (mm)	Young (MPa)	Weight (g)	Area (mm)
1	10	0.1	300	30	1
2	10	0.1	300	8	1
3	10	0.1	300	30	2
4	10	0.2	300	30	1
5	20	0.1	300	30	1
6	20	0.05	1.07	30	1
7	20	0.05	1.07	8	1

Note: the radius of the touch area is listed in the "area" column; the height of chamber is fixed to 3 mm since the results of theoretical analysis imply that it should be as small as possible to improve sensitivity.

ulus of the diaphragm, the thickness of the diaphragm, the size of the touch area, and the weight of the proof mass; with the same configuration, the less the Young's modulus, the thinner the diaphragm, the smaller the touch area, or the heavier the proof mass, and the lower the resonant frequency.

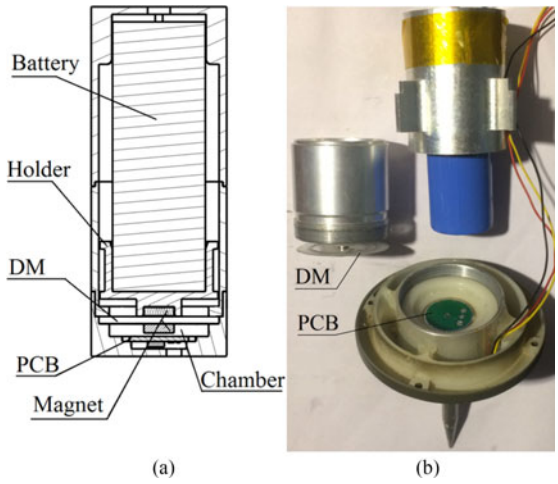

Fig. 5. (a) Schematic section view and (b) the real product of B-VSG.

2) The damping factor is small because there are many spikes in the amplitude of the transfer functions and jumping changes in the phase of the transfer functions.
3) With same Young's modulus, the sensitivities of high frequency are similar between different configurations.
4) Small Young's modulus, such as 1 MPa, means it has more deformation under same air pressure difference between inside and outside of the sealed chamber than the big Young's modulus diaphragm; the smaller the Young's modulus, the lower the sensitivity.
5) From theoretical analysis, the sensitivity is proportional to the initial air pressure of its chamber and is inversely proportional to the height of the chamber.

III. Design and Test

This work has designed and tested two prototypes of VSG. One of them employs a lithium battery as its proof mass and has the name B-VSG. Another one, whose name is M-VSG, uses magnets as its proof mass. These two prototypes both have same structure as Fig. 1 in general, except they have only one diaphragm for the purposes of simplicity. Comparing to two diaphragms, VSG with one diaphragm will be much more unstable when the VSG is not deployed vertically, since the friction between the proof mass and sensor housing will stop the proof mass from vibrating, but the one diaphragm VSG will have better sensitivity at low frequencies because two diaphragms together are thicker than one diaphragm and the thinner one tends to have smaller resonance frequency as shown in Fig. 4.

The prototype B-VSG is made of aluminum and it weighs 33 g where the proof mass, the lithium battery that is about 40 g, is not included. Fig. 5 shows the schematic section view of B-VSG and its real product, in which DM stands for the word "diaphragm." As shown in Fig. 5(a), the chamber is constructed by the diaphragm, parts of housing, and the printed circuit board which has an ICS-40300 MEMS microphone [27] on it. Two magnets fix the holder and the diaphragm with the battery mounted on the holder. Once there is vibration, the battery will force the diaphragm to compress the air in the chamber. The MEMS

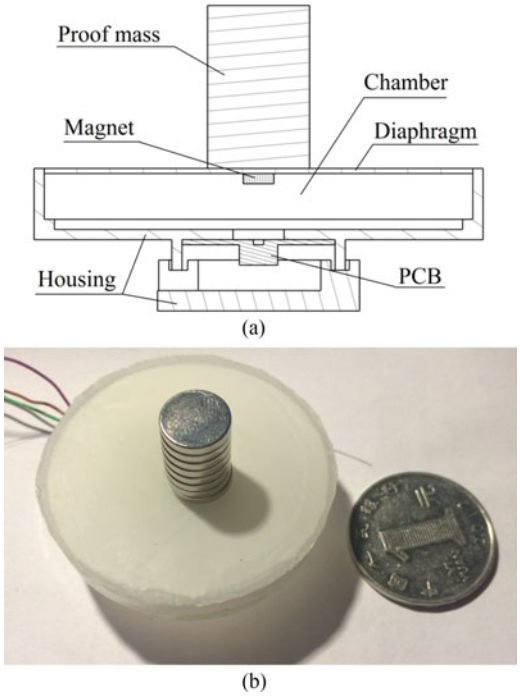

Fig. 6. (a) Schematic section view and (b) the real product of M-VSG.

microphone will measure the local deviation of the air pressure and outputs the vibration in electronic signal. The diaphragm shown in Fig. 5(b) is made of fiberglass and is originally the most important component of stethoscopes to transform the vibration of patient skin into sound wave so as doctors can hear and make diagnoses. More specifically, the Young's modulus of the diaphragm is about 300 MPa, 0.2 mm thick and its effective radius is 10 mm that is equal to the inside radius of the chamber. Thanks to the stiffness of the diaphragm, the chamber can reduce its height to 2.5 mm easily. The diameter of these two magnets determines the size of the touch area whose radius is 1.5 mm as shown in Fig. 5

The prototype M-VSG is made of plastic and weighs 16 g, half of which is contributed by the proof mass. Fig. 6 shows the schematic section view of M-VSG and its real product. M-VSG has the same structure as B-VSG in general, but its diaphragm is made of latex whose Young's modules and thickness are 1.07 MPa and 0.1 mm, respectively. The radius of the proof mass is 5 mm and the height of the chamber is about 6 mm.

The small holes for wire routing on the housing of B-VSG and M-VSG are both sealed by hot-melt adhesive. Transfer functions of these two prototypes are shown in Fig. 7. The resonance frequency of B-VSG is about 70 Hz. It is close to simulation result of configuration 1 in Table I that is 83 Hz and the phase transfer function of B-VSG is similar to configuration 1 too. For M-VSG, one can refer to configuration 7, where radius of touch area is much smaller than M-VSG so the resonance frequency of M-VSG is higher, about 25 Hz. Despite that, the distribution of sensitivity of M-VSG, both in amplitude and phase, is similar to configuration 7 in general. The sensitivity of B-VSG at its resonance frequency is about 33.75 dBV/(m/s) or 60.18 dBV/m

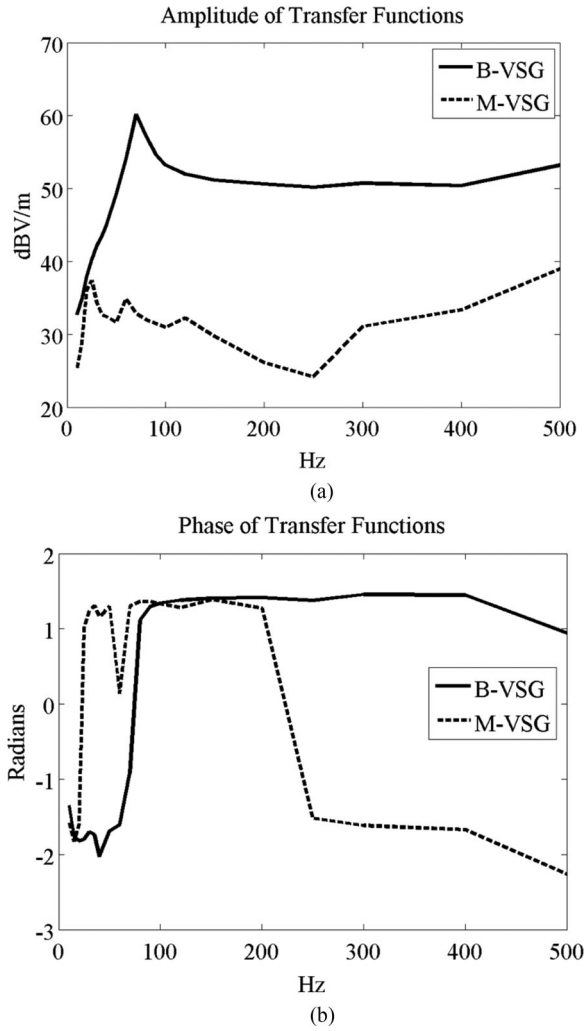

Fig. 7. Transfer functions of prototypes.

which is 58 times of the typical sensitivity of a coil-over-magnet geophone, about 16.07 dBV/(m/s). In fact, from 20 to 500 Hz B-VSG has better sensitivity than the coil-over-magnet geophone, which means B-VSG can replace the geophone to detect seismic targets without severely shortening the detection range.

To test these two prototypes by real seismic waves, a field experiment has been conducted, in which four sensors have been deployed on the side of a mountain path to detect pedestrians. As shown in Fig. 8, these four sensors are a coil-over-magnet geophone, B-VSG, M-VSG, and ICS-40300 MEMS microphone. The coil-over-magnet geophone has resonance frequency at 10 Hz and 16.07 dBV/(m/s) sensitivity. The main job of the MEMS microphone is to recode the sound of the wild environment. All sensors connect to an NI9239 device directly, and the nearby laptop computer records their digitalized signals whose sample rates are 10 kHz through a USB cable. To minimize the interference of wild sounds and winds, four sensors together are covered by a big plastic box after being deployed. Although we are trying to eliminate the sounds in this experiment, they are not always unwanted in the UGS system, since coupled sounds may carry important information for target detection. Except

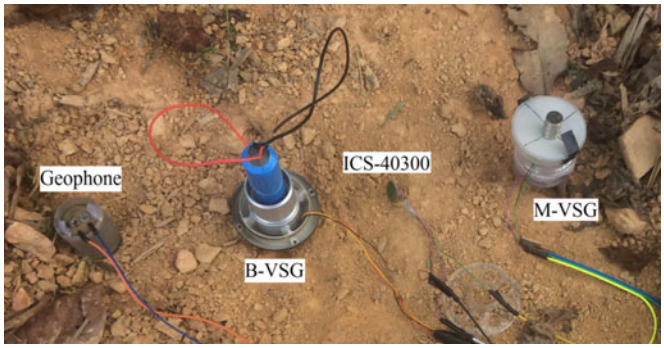

Fig. 8. Four sensors.

TABLE II
SNRs OF FOOTSTEPS

Distance (m)	Geophone (dB)	B-VSG (dB)	M-VSG (dB)	ICS-40300 (dB)
1	20.08	20.59	7.58	7.05
3	13.32	14.39	2.79	2.47
8	5.81	2.10	3.04	3.13
10	3.58	0.52	–1.90	–2.23
13	2.12	–0.34	1.41	1.58

the winds and sounds, another source of noises is the dc-to-dc power supplier, which converts 5 V USB currents into 3.3 V power source and its ripple that is about -42.91 dBV/Hz$^{1/2}$ at 10 Hz will heavily degrade the signal quality of VSGs.

Digital signals from these four sensors are first filtered by a 10–450 Hz band pass filter then down sampled to 1 kHz sample rate. To illustrate the difference between these four sensors, the power spectrum density of background noise and the waveform of a footstep have been shown in Fig. 9. The step was taking a point which is about 1 m away from those sensors. From Fig. 9(a), the coil-over-magnet geophone has the lowest measured background noise since it is a passive device and immune to winds and sounds. The harmonics detected by the geophone come from the fan and hard disk of the data recording laptop computer probably. B-VSG has a thicker housing and a less elastic diaphragm than M-VSG, so B-VSG has lower noise level than M-VSG. Since the sensitivity of M-VSG is low, it measures the sounds of the environment mainly and it has the same background noise level as the ICS-40300 microphone. Examining the short distance single footstep seismic waveform in Fig. 9(b), B-VSG has the biggest amplitude, the geophone seconds while M-VSG and the microphone are just measuring the sound of the step. To compare the coil-over-magnet geophone and B-VSG under different distances, sets of mark time step have been conducted at different distance from sensors. In each set of mark time step, 20 steps have been taken and the average signal noise ratio (SNR), which is calculated by dividing the total energy during the 20 steps by the average energy of the background noise, has been listed in Table II. Since the background noise level of VSGs is high at low frequencies, and the B-VSG has better sensitivity since 20 Hz, the digital signals of VSGs and microphone are further filtered by a 20 Hz high pass filter. The SNRs of M-VSG and microphone in Table II

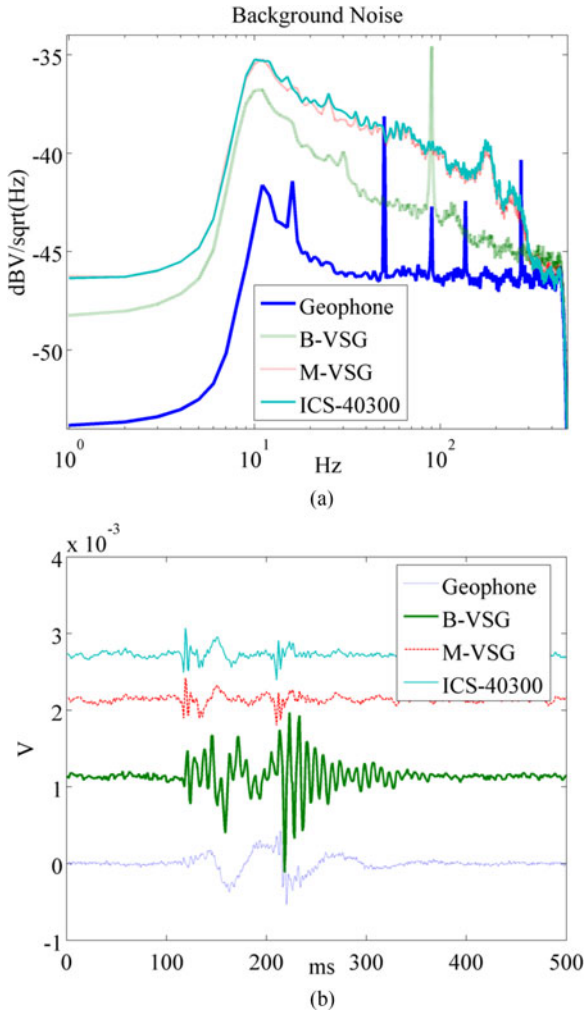

Fig. 9. (a) Power spectrum density of background noise and (b) the wave forms of a footstep.

below 3 m (not included) are not correctly implying that the noise has already covered the sound of those footsteps. When the distance increases to 13 m, B-VSG cannot detect the footsteps while the coil-over-magnet geophone still has high SNR. This is mainly because seismic waves will keep their low frequency components during propagations [17] and the geophone has lower resonance frequency than B-VSG. So, to increase the detect radius of B-VSG, one should decrease its resonance frequency by increasing the weight of the battery, increasing the radius of the diaphragm, reducing the Young's modules of diaphragm, and (or) decreasing the radius of the touch area.

IV. CONCLUSION

A new kind of vibration sensor was introduced in this work, which consisted two components, a vibration to sound mechanism and a microphone. First, the mechanism converted vibration energy into sound. Second, the microphone measured the generated sound and outputted electricity signal that was the final output of the vibration sensor. Since the working principle of the vibration sensor is converting vibration into sound, the

vibration sensor got the name: VSG. According to the theoretical analysis, the sensitivity of VSG was inversely proportional to the height of its chamber, and was proportional to its initial air pressure. The results of simulation pointed out that the radius, thickness, and Young's modulus of the elastic diaphragm, the weight of the proof mass, the size of the touch area between the proof mass and the diaphragm, all together were controlling the resonance frequency of VSGs. In addition, a diaphragm with too small Young's modulus will heavily degrade the sensitivity since it usually has too much deformation under same air pressure.

The prototype B-VSG took the battery of the wireless sensor node as its proof mass, so as it had sensitivity of 60.18 dBV/m at 70 Hz, which was 58 times of the sensitivity of the coil-over-magnet geophone, and only weighed 33 g that was half of the weight of the coil one. In addition, its rated power was lower than 726 μW, which was far more energy efficient than MEMS accelerators and molecular-electronic transducers. The field test of VSGs showed that although VSGs suffered a lot from winds, sounds, and power source, the prototype B-VSG still had similar detect ability as the coil-over magnet geophone within 10 m from seismic source. To increase the cover range of B-VSG, the suggestions were as follows.

1) Increase the weight of the battery.
2) Enlarge the surface of the elastic diaphragm.
3) Decrease the thickness and Young's modulus of the diaphragm carefully.
4) Shrink the size of the touch area.
5) Decrease the height of the chamber.
6) Make sure there was no friction that stopped the proof mass from vibrating and used low noise power source.

Currently, B-VSG can detect seismic waves from 20 to 500 Hz or even higher. For seismic waves lower than 20 Hz, we are following up-mentioned six suggestions and may eventually get a light, stable, and robust VSG that resonates at 10 Hz in one or two years. By then, the VSG will be highly integrated into our wireless sensor node with battery and other sensors as its proof mass all together.

For further evolution, by combining VSG and MEMS technology, VSG may become a new kind of MEMS vibration sensor, with similar sensitivity as the coil-over-magnet geophone, size and energy efficiency as MEMS microphones.

References

[1] K. E. Speller and D. Yu, "A low-noise MEMS accelerometer for unattended ground sensor applications," *Proc. SPIE, Int. Soc. Opt. Eng.*, vol. 5417, pp. 63–72, 2004.

[2] J. Lan, S. Nahavandi, T. Lan, and Y. Yin, "Recognition of moving ground targets by measuring and processing seismic signal," *Measurement*, vol. 37, pp. 189–199, 2005.

[3] J. H. Lan, T. Lan, and S. Nahavandi, "A novel application of a microaccelerometer for target classification," *IEEE Sensors J.*, vol. 4, no. 4, pp. 519–524, Aug. 2004.

[4] R. Ghosh, A. Akula, S. Kumar, and H. K. Sardana, "Time–frequency analysis based robust vehicle detection using seismic sensor," *J. Sound Vib.*, vol. 346, pp. 424–434, 2015.

[5] K. Dai, X. Li, C. Lu, Q. You, Z. Huang, and H. F. Wu, "A low-cost energy-efficient cableless geophone unit for passive surface wave surveys," *Sensors*, vol. 15, pp. 24698–24715, 2015.

[6] P. Anghelescu, G. V. Iana, and I. Tramandan, "Human footstep detection using seismic sensors," in *Proc. Int. Conf. Electron., Comput. Artif. Intell.*, 2015, pp. 1–5.

[7] Q. Zhou, G. Tong, D. Xie, B. Li, and X. Yuan, "A seismic-based feature extraction algorithm for robust ground target classification," *IEEE Signal Process. Lett.*, vol. 19, no. 10, pp. 639–642, Oct. 2012.

[8] Q. Zhou *et al.*, "A quarter-car vehicle model based feature for wheeled and tracked vehicles classification," *J. Sound Vib.*, vol. 332, pp. 7279–7289, 2013.

[9] M. Hons, R. Stewart, D. Lawton, and M. Bertram, "Ground motion through geophones and MEMS accelerometers: Sensor comparison in theory, modeling, and field data," *SEG Tech. Program Expanded Abstracts*, vol. 26, pp. 1–5, 2013.

[10] COLIBRYS SF1500S.A / SF1500SN.A, accessed on Aug. 17, 2016, [Online]. Available: http://www.treffer.com.br/produtos/Colibrys/pdf/DS SF1500A.30S.SF1500A.E.06.10.pdf

[11] H. Wang, W. Quan, Y. Wang, and G. R. Miller, "Dual roadside seismic sensor for moving road vehicle detection and characterization," *Sensors*, vol. 14, pp. 2892–2910, 2014.

[12] H. Jo, J. A. Rice, and B. F. Spencer, "Development of high-sensitivity accelerometer board for structural health monitoring," *SPIE Smart Struct. Mater. Nondestruct. Eval. Health Monit.*, vol. 7647, 2010, Art. no. 764706.

[13] R. Levy, G. Papin, O. L. Traon, D. Janiaud, and J. Guerard, "Nonlinear regime operation for a high resolution vibrating beam UGS seismometer," *Analog Integr. Circuits Signal Process.*, vol. 82, pp. 621–626, 2015.

[14] Analog devices ADXL206, accessed on Aug. 17, 2016, [Online]. Available: http://www.analog.com/media/en/technical-documentation/data-sheets/ADXL206.PDF

[15] Compact molecular-electronic seismic sensors, accessed on Aug. 19, 2014, [Online]. Available: http://r-sensors.ru/1_products/Compact_seismic_sensors_MTSS.pdf

[16] MT LA-2050 Sensor, accessed on Dec. 20, 2016, [Online]. Available: http://static1.1.sqspcdn.com/static/f/658572/9280948/1288962644393/MTLA-2050.pdf?token=iQvEYcztlEY6zUqm4PMSqM5azD8%3D

[17] V. V. Krylov, S. Pickup, and J. McNuff, "Calculation of ground vibration spectra from heavy military vehicles," *J. Sound Vib.*, vol. 329, pp. 3020–3029, Jul. 2010.

[18] J. Altmann, "Acoustic and seismic signals of heavy military vehicles for co-operative verification," *J. Sound Vib.*, vol. 273, pp. 713–740, 2004.

[19] M. A. Lak, G. Degrande, and G. Lombaert, "The effect of road unevenness on the dynamic vehicle response and ground-borne vibrations due to road traffic," *Soil Dyn. Earthq. Eng.*, vol. 31, pp. 1357–1377, Oct. 2011.

[20] J. Huang, Q. Zhou, X. Zhang, E. Song, B. Li, and X. Yuan, "Seismic target classification using a wavelet packet manifold in unattended ground sensors systems," *Sensors*, vol. 13, pp. 8534–8550, 2013.

[21] A. A. Dibazar, S. George, and T. W. Berger, "Statistical spiking model for real world pattern recognition applications," in *Proc. Int. Joint Conf. Neural Netw.*, 2010, pp. 1–4.

[22] J. M. Sabatier and A. E. Ekimov, "Range limitation for seismic footstep detection," *SPIE Proc., Unattended Ground, Sea, Air Sens. Technol. Appl.*, vol. 6963, 2008, Art. no. 69630V.

[23] G. Succi, D. Clapp, R. Gampert, and G. Prado, "Footstep detection and tracking," *Proc. SPIE*, vol. 4393, pp. 22–29, 2001.

[24] L. Zhi-Qiang, W. E. I. Jian-Ming, Z. Jun-Yu, and L. I. U. Hai-Tao, "Algorithm for person footstep detection and identification of seismic signal based on Egent-ropy," *Mini Micro Syst.*, vol. 31, pp. 190–192, 2010.

[25] G. E. Sleefe, M. D. Ladd, T. S. McDonald, and G. J. Elbring, "Acoustic and seismic modalities for unattended ground sensors," *Unattended Ground Sens. Technol. Appl.*, vol. 3713, pp. 2–9, 1999.

[26] R. Brincker, T. L. Lagö, P. Andersen, and C. Ventura, "Improving the classical geophone sensor element by digital correction," in *Proc. IMAC-XXIII, Conf. Expo. Struct. Dyn.*, 2005, pp. 1–9.

[27] InvenSense ICS-40300, accessed on Aug. 17, 2016, [Online]. Available: https://store.invensense.com/datasheets/invensense/ICS-40300_ProductSpec_V1 0.pdf

Qianwei Zhou (A'17) received the Ph.D. degree in communication and information systems from the Shanghai Institute of Microsystem and Information Technology, University of Chinese Academic and Sciences, Shanghai, China, in 2014.

In July 2014, he joined Zhejiang University of Technology, Hangzhou, China, where he is currently a Research Scientist in the College of Computer Science. He has published more than ten scientific papers in international journals and conference proceedings, including the IEEE SIGNAL PROCESSING LETTERS, IEEE TRANSACTIONS ON MAGNETICS, IEEE TRANSACTIONS ON INSTRUMENTATION AND MEASUREMENT, and *Journal of Sound and Vibration*. His research interests include the crossing field of machine learning and computer-aided design, Internet-of-Thing-related signal processing, and pattern recognition.

Baoqing Li received the Ph.D. degree in MEMS systems from the State Key Laboratory of Transducer Technology, Shanghai Institute of Metallurgy, Chinese Academy of Sciences, Shanghai, China, in 1999.

In March 2006, he joined the Shanghai Institute of Microsystem and Information Technology, Chinese Academy of Sciences, Shanghai, China, where he is currently a Professor and a Tutor of Ph.D. students in the area of wireless sensor networks. From 2001 to 2005, he was with the Center of Microelectronics, New Jersey Institute of Technology, Newark, NJ, USA, working with a focus on applications of MEMS technology.

Huawei Liu received the M.S. degree in underwater acoustics engineering from Harbin Engineering University, Harbin, China, in 2008. Currently, he is working toward the Ph.D. degree in communication and information systems at the Shanghai Institute of Microsystem and Information Technology, Chinese Academy of Sciences, Shanghai, China.

He joined the Shanghai Institute of Microsystem and Information Technology, Chinese Academy of Sciences, in April 2008. He is currently a Research Assistant in the Science and Technology on Microsystem Laboratory, Shanghai Institute of Microsystem and Information Technology, Chinese Academy of Sciences. His research interests include signal processing of array sensors, moving object detection, and recognition.

Shengyong Chen (M'01–SM'10) received the Ph.D. degree in computer vision from the City University of Hong Kong, Hong Kong, in 2003.

He is currently a Professor with Tianjin University of Technology, Tianjin, China, and Zhejiang University of Technology, Hangzhou, China. He received a fellowship from the Alexander von Humboldt Foundation of Germany and worked at the University of Hamburg in 2006–2007. He has published more than 100 scientific papers in international journals. His research interests include computer vision, robotics, and image analysis.

Prof. Chen received the National Outstanding Youth Foundation Award of China in 2013. He is a Fellow of the Institution of Engineering and Technology, U.K., and a Senior Member of the China Computer Federation.

Jingchang Huang received the Ph.D. degree in communication and information systems from the University of Chinese Academic and Sciences, Beijing, China, in 2015.

In 2015, he joined IBM-Research, Shanghai, China, where currently he is a Research Scientist on the Cognitive-IOT team. He has developed some efficient algorithms of target detection and classification for unattended ground sensors systems and published papers on them in IEEE TRANSACTIONS and journals. He mainly focuses on cognitive signal processing, including but not limited to acoustic, image, air quality data, all of which comes from Internet-of-Thing-related applications. His current research interests also include pattern recognition, big data, and wireless sensor networks.